Technical University of Denmark

DTU

Calculated stacking-fault energies of elemental metals

Rosengaard, N. M.; Skriver, Hans Lomholt

DTU Library
Technical Information Center of Denmark

Calculated stacking-fault energies of elemental metals

N. M. Rosengaard and H. L. Skriver

Physics Department, Technical University of Denmark, DK-2800 Lyngby, Denmark

We have performed *ab initio* calculations of twin, intrinsic, and extrinsic face-centered-cubic stacking faults for all the 3*d*, 4*d*, and 5*d* transition metals by means of a Green's-function technique, based on the linear-muffin-tin-orbitals method within the tight-binding and atomic-sphere approximations. The results are in excellent agreement with recent layer Korringa-Kohn-Rostoker Green's-function calculations where stacking-fault energies for Ni, Cu, Rh, Pd, Ag, Ir, and Au were found by means of the the so-called force theorem. We find that the self-consistent fault energies for all the metals in the three transition series vary with atomic number essentially as the calculated structural energy differences between the face-centered-cubic and the hexagonal-close-packed phases. In addition we find that the simple relationships between the different types of fault energies predicted by models based on the local atomic coordination are obeyed to a high degree of accuracy.

I. INTRODUCTION

The face-centered-cubic (fcc) and the hexagonal-close-packed (hcp) crystal structures of metals may be regarded as the stacking of layers of hexagonally arranged atoms. Symbolically these structures may be represented by the stacking sequences $ABCABC$ and $ABABAB$, respectively, which indicate the position of the nearest neighbors in adjacent layers. In real metals these perfect stacking sequences may be broken locally by the introduction of one of the three stacking faults shown in Fig. 1, and this effect is of great importance in determining crystal growth, dislocation motion, and deformation processes in general.

The intrinsic fault is the stacking fault most commonly found in experiments on fcc metals and it may be represented by the stacking sequence $CABC \mid BCAB$, where $\mid$ denotes a symmetry plane of the resulting fault sequence. One may arrive at this fault by the removal

FIG. 1. Stacking sequence of the fcc and hcp crystal structures together with those of the twin, intrinsic, and extrinsic stacking faults. The stacking sequences are represented by lines between nearest neighbors in adjacent layers. Filled circles represent atoms in layers of the local hcp environment. Interlayer structure constants are labeled according to the environment of the neighboring layer.

of a layer labeled A at the position of the symmetry plane. A more physical operation which also produces the intrinsic fault is the application of the shearing operation given by the vector $\frac{1}{6}[\bar{2}11]$ to the part of the perfect crystal on the right-hand side of an arbitrary atomic layer. This operation causes the transformations $A \rightarrow B$, $B \rightarrow C$, and $C \rightarrow A$ and, hence, produces the intrinsic sequence. The extrinsic fault may be formed by applying the same shearing operation to a crystal containing an intrinsic fault. In this case the shearing of planes more than one atomic layer to the right of the symmetry plane of the intrinsic fault produces the extrinsic sequence $ABCBABC$. The twin fault may be assigned the sequence $ABCBA$ in the above notation and in contrast to the intrinsic and extrinsic faults, which are planar defects in a perfect crystal, the twin fault is simply the plane boundary between two crystalline grains with fcc stacking sequences of different orientation.

Experimentally, stacking faults are observed in connection with the splitting of dislocations into partials. In this process the energy cost of forming the fault will oppose the energy gained by moving the partials apart, leading to an equilibrium distance of dissociation of the partials. The stacking-fault energies obtained in the study of the dissociation of dislocations as well as by other experimental means are summarized by Hirth and Lothe.[1] Unfortunately, the precise determination of stacking-fault energies is difficult, especially for materials with large stacking-fault energies, because the separation between partials is inversely proportional to the fault energy. Therefore the experimentally determined fault energies have errors of unknown magnitude.

From a theoretical point of view, twin and stacking faults in close-packed metals represent well-defined planar defects, and the determination of their energy of formation by *ab initio* calculations is an appropriate starting point for macroscopic models of mechanical properties. In addition, comprehensive theoretical studies of stacking faults may serve to establish simple trends in
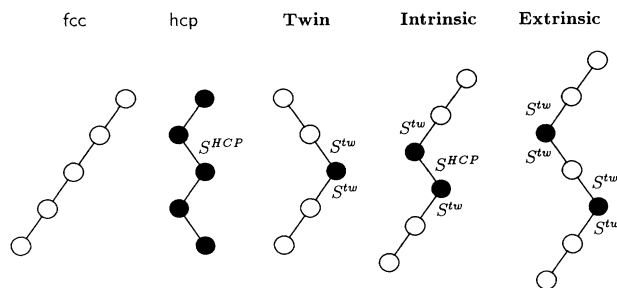
the energies and thereby be used to systematize the existing experimental data. The first *ab initio* calculations of stacking-fault energies for most of the elemental fcc metals were performed by Crampin et al.[2] who found that, although their calculated energies were generally somewhat higher than the experimental values, they gave a correct description of the trends observed experimentally. Other local-density calculations on selected fcc metals include those of Denteneer and Soler,[3] Xu, Lin, and Freeman,[4] Schweizer et al.,[5] Fähnle et al.,[6] Wright, Daw, and Young,[7] and Hammer et al.[8]

In the present paper, we report a series of *ab initio* calculations of stacking-fault energies in elemental 3d, 4d, and 5d transition and noble metals by means of a linear-muffin-tin-orbitals (LMTO) Green's-function technique[9] within the atomic-spheres approximation (ASA). The technique has recently been successfully applied in calculations of work functions and surface energies of a large number of elemental metals[10,11] including the magnetic 3d transition metals.[12] In contrast to the formation of a surface, the introduction of stacking faults conserves the number of nearest-neighbor bonds. Hence, stacking-fault energies are typically one order of magnitude smaller than the corresponding surface energies and their calculation requires a high numerical accuracy in terms of dense k-vector and energy samplings. On the other hand, the perturbations in the neighborhood of a stacking fault are generally small and, in particular, the close packing of atoms is conserved. As a result, the errors of the physical approximations in the ASA are minimal, and we expect the Green's-function technique to yield accurate stacking-fault energies.

II. COMPUTATIONAL METHOD

Our tight-binding LMTO Green's-function technique[9] is based on the work by Andersen and co-workers.[13-19] An essential aspect of the technique is the ability, within the ASA and in the tight-binding representation, to generate the Green's-function matrices for a real, two-dimensional interface by a simple and efficient procedure. The details of the technique may be found in Ref. 9. Here, we shall restrict ourselves to an outline of the major steps, with special emphasis on the derivation of the Green's-function matrix for a stacking fault. In addition, we shall discuss a development in which the linearized Dyson equation is used to reduce the computer time involved in the self-consistency procedure.

A. The LMTO Green's-function formalism

The Green's-function technique, which we use to solve the one-electron problem, exploits the relation between the eigenvalue equations defined by the LMTO-ASA Hamiltonian H^γ in the nearly orthogonal γ representation and the solution of the Korringa-Kohn-Rostoker (KKR)-ASA equations in the most localized tight-binding β representation. To second order in $(\epsilon - \epsilon_\nu)$, where ϵ_ν is an arbitrary energy in the energy range of interest, the Hamiltonian Green's function G^γ may be obtained from the LMTO-ASA equation

$$[z\mathbf{1} - H^\gamma]G^\gamma(z) = 1. \tag{1}$$

Here, z is a complex energy and

$$H^\gamma = C + \sqrt{\Delta}S^\gamma\sqrt{\Delta}, \tag{2}$$

the LMTO Hamiltonian written in terms of structure constants S^γ and center C, bandwidth Δ, and γ potential parameters. The KKR-ASA Green's function g^β is defined in terms of the KKR-ASA equation

$$[P^\beta(z) - S^\beta]g^\beta(z) = 1, \tag{3}$$

where P^β is a diagonal potential-function matrix, the elements of which obey the scaling relation

$$(P^\beta)^{-1} + \beta = (P^\gamma)^{-1} + \gamma \tag{4}$$

and S^β is a structure constant matrix which may be evaluated in real space. Within the nearly orthogonal representation, the potential function is linear in energy, i.e.,

$$P^\gamma(z) = \frac{z - C}{\Delta}, \tag{5}$$

and as a result the Hamiltonian Green's function G^γ and the KKR-ASA Green's function g^γ are connected by the simple scaling relation

$$G^\gamma(z) = \Delta^{-1/2}g^\gamma(z)\Delta^{-1/2}. \tag{6}$$

The transformation of the KKR-ASA Green's function between different representations has the form[16,18]

$$g^\gamma(z) = (\gamma - \beta)\frac{P^\beta(z)}{P^\gamma(z)} + \frac{P^\beta(z)}{P^\gamma(z)}g^\beta(z)\frac{P^\beta(z)}{P^\gamma(z)}, \tag{7}$$

where β and γ are the diagonal screening constant and potential parameter matrices, respectively.

In the calculation of the Green's function for an interface, we exploit the short range of the most localized structure constants to get matrix equations of finite dimension. Hence, we calculate g^β from the relevant Dyson equations. On the other hand, the charge density needed in a self-consistent calculation is most conveniently obtained in terms of one-center expansions and partial-wave-projected state densities. For this purpose we need the imaginary part of the Hamiltonian Green's function G^γ and this we obtain from g^β by means of the scaling relations Eqs. (6) and (7). We point out that these scaling relations are given in terms of diagonal matrices and hence are extremely efficient in numerical calculations.

B. Green's functions for stacking faults

The starting point for the Green's-function technique is the self-consistent one-electron potential of the perfect crystal, from which one proceeds to account for the changes in potential and structure near the interface by means of Dyson's equation. In the case of a general interface, one first inhibits hopping across the interface plane and constructs the so-called ideal Green's function,[20] $\tilde{g}$. This Green's function represents a perfect crystal terminated not by a hard-wall potential but by $P^\beta = \infty$, corresponding roughly to a vacuum potential lying 1 Ry above

the occupied bands.[19] Next, one uses Dyson's equation, which includes the structural changes in terms of structure constant differences, to obtain the ideal Green's functions for the fault structure. After that, the left- and right-hand ideal Green's functions are reconnected to form the Green's function for the complete fault structure with unrelaxed potentials. Finally, the potentials are relaxed and the Green's function is iterated to self-consistency.

Let A denote layers on the left-hand side, and B layers on the right-hand side of the interface. In this notation the KKR-ASA ideal Green's-function matrix for the left half-space is defined by

$$[P_A(z) - S_{AA}(\mathbf{k}_{||})]\tilde{g}_{AA}(\mathbf{k}_{||}, z) = 1, \tag{8}$$

where $\mathbf{k}_{||}$ is the label of the two-dimensional (2D) Bloch representation. Here and in the following we suppress the LMTO tight-binding representation label β. In the original implementation[9] the ideal Green's-function matrix was obtained by means of a $\mathbf{k}_\perp$ integration of the Green's-function matrix for the perfect crystal. This integration turned out to be a time-consuming process, especially for the high accuracy needed in the calculation of stacking-fault energies, and instead we have now introduced the notion of principal layers[21] which was recently implemented by Kudrnovsky and co-workers.[22,23]

A principal layer[21] is defined as the minimum number of atomic layers which ensures that hopping only occurs between nearest-neighbor principal layers. In the KKR-ASA equations, the range of the hopping is determined by the structure constants, and as a result of the short range within the tight-binding representation, a principal layer typically consists of only two atomic layers. To derive the central equation of the principal-layer technique one considers the situation in which a principal layer is added to a surface described by an ideal Green's function. From the Dyson equation connecting the Green's function $\bar{g}$, with hopping between the semi-infinite crystal and the added layer and the Green's function $\tilde{g}$, without this hopping, one arrives at the equation given by Kudrnovsky and Drchal[22]

$$\bar{g}_{00}(\mathbf{k}_{||}, z) = [\, P_0(z) - S_{00}(\mathbf{k}_{||})$$
$$- S_{01}(\mathbf{k}_{||})\tilde{g}_{11}(\mathbf{k}_{||}, z)S_{10}(\mathbf{k}_{||})]^{-1}, \tag{9}$$

which is analogous to Eq. (41) in Ref. 9 where a complete half-space and not just a single principal layer was added.

In the principal-layer equation (9) the index 0 represent the added principal layer and the index 1 represent the top principal layer of the original semi-infinite crystal. Furthermore, $\bar{g}_{00}$ is the ideal Green's function projected on the added principal layer, $\tilde{g}_{11}$ is the Green's function without hopping projected on the original top principal layer, and the hopping is mediated by the structure constants S_{10} and S_{01} connecting the added layer and the original top layer. Now, the introduction of the hopping makes the added principal layer identical to the top principal layer of a semi-infinite crystal, and it follows that $\tilde{g}_{11}(\mathbf{k}_{||}, z) = \bar{g}_{00}(\mathbf{k}_{||}, z)$. This identity may be introduced into Eq. (9) which then becomes a quadratic equation in $\tilde{g}_{11}$, i.e., $\tilde{g}_{AA}$ in the notation of Eq. (8), that may be

solved by iteration.

In the most localized representation one may calculate the 2D structure constants directly as the Bloch sum

$$S^\beta_{RL,R'L'}(\mathbf{k}_{||}) = \sum_{\mathbf{T}_{||}} e^{i\mathbf{k}_{||}\cdot\mathbf{T}_{||}} S^\beta_{RL,R'+\mathbf{T}_{||}L'} \tag{10}$$

in real space. Here L denotes angular momentum, R a 2D basis vector, $S^\beta_{RL,R'+\mathbf{T}_{||}L'}$ the transfer matrices connecting sites R and R' in the 2D basis, and $\mathbf{T}_{||}$ a 2D translation vector. The transfer matrices are in turn defined by the matrix equation

$$S^\beta = S^o + S^o \beta S^\beta, \tag{11}$$

where S^o is the conventional LMTO transfer matrix and β is the diagonal screening matrix given by Andersen and co-workers.[16,18] The most localized transfer matrices are obtained from this equation by inversion on a sufficiently large cluster of neighboring atomic sites.

Once the ideal Green's-function matrices $\tilde{g}_{AA}$ and $\tilde{g}_{BB}$ for the two semi-infinite sides of the interface have been calculated by means of Eq. (9), the rearrangement of sites corresponding to the stacking fault may be introduced separately in the two half spaces. Thus, we calculate the ideal Green's-function matrix for the left-hand side of the fault structure $\tilde{g}^f_{AA}$ by Dyson's equation

$$[1_{AA} - \tilde{g}_{AA}\Delta S^f_{AA}]\tilde{g}^f_{AA} = \tilde{g}_{AA}, \tag{12}$$

and the Green's-function matrix for the right-hand side by the analogous equation. In Eq. (12) the perturbation is the change in the structure constant matrix for the A side

$$\Delta S^f_{AA} = S^f_{AA} - S_{AA}, \tag{13}$$

which is finite and may be calculated directly in real space. The hopping between the two sides of the fault structure may be introduced through the equation

$$\left(\begin{bmatrix} 1_{AA} & 0_{AB} \\ 0_{BA} & 1_{BB} \end{bmatrix} + \begin{bmatrix} \tilde{g}^f_{AA}(z) & 0_{AB} \\ 0_{BA} & \tilde{g}^f_{BB}(z) \end{bmatrix} \begin{bmatrix} 0_{AA} & S^f_{AB} \\ S^f_{BA} & 0_{BB} \end{bmatrix}\right) g(z)$$

$$= \begin{bmatrix} \tilde{g}^f_{AA}(z) & 0_{AB} \\ 0_{BA} & \tilde{g}^f_{BB}(z) \end{bmatrix}, \tag{14}$$

where the structure constant matrices that connect the two sides are those of the fault structure. This equation is analogous to Eq. (36) of Ref. 9 and may be solved in a similar manner. The result is the Green's-function matrix for the fault structure with unrelaxed potential functions.

In a self-consistency procedure, g provides the first guess at the self-consistent Green's-function matrix g^i, determined by succesive solution of the Dyson equation

$$[1 + g(z)\Delta P^i(z)]g^i(z) = g(z), \tag{15}$$

where $\Delta P^i(z) = P^i - P$ is the relaxation that occurs in the potential function close to the fault structure. The solution of the Dyson equation for the KKR-ASA Green's function has the advantage that the potential enters only through changes in the diagonal potential-function ma-

trix. Therefore the dimension of the Dyson equation is determined by the small number of atomic spheres with nonvanishing $\Delta P^i(z)$, i.e., with a perturbed potential. This is in contrast to the case of the Hamiltonian formalism, where the relaxation of the potentials enters as changes in the nondiagonal elements of the Hamiltonian and overlap matrices and may be of long range.

The KKR-ASA Green's function (15) in the tight-binding representation may be scaled to the second-order Hamiltonian Green's function G^γ as explained in Sec. II A. This latter Green's function is directly related to the partial-wave projected state density and yields the moments of the state density by the integral

$$m_{RL}^q = \frac{1}{\pi}\mathrm{Im}\int_{\cup E_F} dz\, z^q \int_{\mathrm{BZ}} d^2 k_{||} G_{RL,RL}^\gamma(k_{||}, z),\qquad (16)$$

where the energy integration is performed on a contour in the lower half-plane cutting the real axis at the Fermi level E_F, and the $k_{||}$ integration extends over the 2D Brillouin zone. In the actual self-consistent calculations, only the first few moments $q = 0, 1, 2$ obtained by Eq. (16) from the site- and L-diagonal elements of the Green's-function matrix are needed since they contain all the electronic-structure information necessary to calculate the electron density and total energies within the ASA.

C. Linearized Dyson equation

In the interface Green's-function technique the computer time is dominated by the solution of Dyson's equation (15) for the relaxed potentials. It is therefore desirable, especially in systematic studies of several systems, to reduce the number of times the complete Dyson equation must be solved. In the following, we shall describe how a reduction by almost one order of magnitude may be accomplished by a linearization of the Dyson equation and the calculation of a few nondiagonal state-density moments.

Let us assume that we have solved the Dyson equation (15) for a specified potential. Hence, we know the moments of the state density from the contour integral (16). If we now add a perturbation δH^γ to the LMTO Hamiltonian G^γ, the corresponding first-order change in the Green's function may be found from

$$\delta G^\gamma(z) = G^\gamma(z)\delta H^\gamma G^\gamma(z),\qquad (17)$$

as obtained by keeping terms to linear order in (1). The perturbation of the Hamiltonian caused by a change in the potential may be written in terms of the corresponding change in the potential parameters and if we keep only the dominant contribution we have $\delta H^\gamma = \delta C$ where C is the band center. Hence, to leading order the change in the Green's function is

$$\delta G^\gamma(z) = G^\gamma(z)\delta C G^\gamma(z).\qquad (18)$$

It is also possible to include the changes in the bandwidth parameter Δ and the band distortion parameter γ, but experience shows that these are normally not needed.

We may now insert (18) into (16) to obtain the linear change in the moments caused by the change in potential expressed through the shift in the band centers. We find

$$\delta m_{RL}^q = \sum_{R'L'} \frac{\partial m_{RL}^q}{\partial C_{R'L'}}\delta C_{R'L'},\qquad (19)$$

$$\frac{\partial m_{RL}^q}{\partial C_{R'L'}} = \frac{1}{\pi}\mathrm{Im}\int_{\cup E_F} dz\, z^q$$
$$\times \int_{\mathrm{BZ}} d^2 k_{||} G_{RLR'L'}^{\gamma k_{||}}(z)G_{R'L'RL}^{\gamma k_{||}}(z)\qquad (20)$$

from which it is seen that the integrations over k space and along the energy contour need only be done once for a given solution of the exact Dyson equation, $G^{\gamma k}(z)$. Hence, within the linear approximation the moments corresponding to a relaxed potential are simply given by adding δm_{RL}^q to the already known moments.

D. Self-consistency procedure

The starting point for the iterations towards self-consistency is formed by the perfect interface Green's function (14) corresponding to unrelaxed bulk potentials, which at the outset gives state-density moments (16) and their parameter derivatives (20). With this information, one may perform an approximate self-consistency cycle in which (19) is used to calculate the charge densities needed in the solution of Poisson's equation. Once self-consistency has been reached within the linear approximation to Dyson's equation, the reference Green's function may be updated by solving the exact Dyson equation, and a new approximate cycle started. In this manner, one succesively eliminates second- and higher-order contributions to the self-consistent interface Green's function.

We find that the series of Green's functions and one-electron potentials generated in our two-step procedure is rapidly convergent. As a result, the number of times the exact, time-consuming Dyson equation must be solved is reduced to a minimum. In the present calculations typically 4–5 updates of the Green's-function matrices were necessary while for surface calculations[11] where the perturbations in the potentials were substantial the number of updates goes up to 8–10.

E. Details of the calculations

At the outset of a stacking-fault calculation, one needs starting potentials as well as total energies corresponding to the perfect, infinite crystal of the atomic species that form the fault structure. To obtain this input, we perform self-consistent bulk calculations by means of the second-order Hamiltonian (2), and calculate the one-electron contribution to the kinetic energy by integrating the bulk Green's function on a complex energy contour. The contour is chosen as a semicircle and the integration performed by a Gaussian technique on a mesh of 25 points distributed exponentially so as to increase the

TABLE I. Twin-fault energy in (mRy) for the fcc transition metals calculated with two sampling densities in the irreducible part of the 2D Brillouin zone.

$k_{\parallel}$	Ni	Cu	Rh	Pd	Ag	Ir	Pt	Au
45	2.14	0.78	4.45	3.08	0.61	6.51	5.88	0.79
135	2.18	0.67	4.17	3.20	0.54	6.34	5.47	0.85

sampling density near the Fermi level. Furthermore, although it is more time consuming, we use in the bulk calculations a Brillouin zone based on the 2D zone of the fault structure, and in the direction perpendicular to the plane of the 2D zone we use 400 k points distributed over the period $2\pi/d_{\perp}$, where $d_{\perp}$ is the distance between the fault planes. This large number is necessary because the Green's functions for the fault structures are calculated by the principal-layer technique, and hence is completely converged in terms of $\mathbf{k}_{\perp}$.

Based on convergence tests, the fault calculations are performed using a fault region consisting of seven layers for the twin fault, eight layers for the intrinsic fault, and nine layers for the extrinsic fault. For the $\mathbf{k}_{\parallel}$ integration we use 135 special points[24] in the irreducible part of the two-dimensional hexagonal Brillouin zone. As indicated by the results in Table I, a less dense sampling leads to errors of up to 15%. Furthermore, to maintain charge neutrality the small excess charge ($< 10^{-3}$ electrons) of the fault region is placed at two sheets just outside the fault structure, and the corresponding contribution to the one-electron potential and the total energy are included. In this manner, we take approximate account of the charge connected with the Friedel oscillations and ensure fast convergence of the fault energies in terms of the region size. Finally, for exchange and correlation we use the local-density functional of Ceperley and Alder[25] as parametrized by Perdew and Zunger.[26]

III. RESULTS

In the following we shall present twin, intrinsic, and extrinsic face-centered-cubic stacking-fault energies for 28 elemental metals, as obtained by the procedure described in Sec. II. All calculations are performed at 0 K and at the experimentally observed equilibrium volumes, and structural relaxations are neglected. The results are listed in Tables II–V and compared with other *ab initio* calculations as well as available experimental data.

A. The face-centered-cubic metals

Out of the 28 metals treated here only nine form naturally in the fcc structure, and for these we have collected available values for the stacking-fault energies in Tables II–IV. It is seen that the present results give a correct description of the trend observed experimentally and that they generally are higher than the corresponding experimental values, the only exception being the intrinsic fault energy in Rh. We find this agreement satisfactory, especially in view of the large uncertainties connected with the experimental determination.

There are a number of *ab initio* calculations of stacking-fault energies with which to compare, the most comprehensive being those of Crampin *et al.*[2] These authors used the LKKR Green's-function method[27] in conjunction with the so-called force theorem. Thus, they apply frozen bulk potentials and obtain a stacking-fault energy as the difference in the sum of the one-electron energies between the fault structure and the perfect crystal to which they add a term proportional to the excess charge in the fault region. The procedure is not self-consistent but is expected to work well, as indeed the results indicate it does.

TABLE II. Twin-fault energy for the fcc transition metals.

		E_{twin} (mJ/m^2)				
Metal	APW[a]	Supercell pseudo[b]	LMTO[c]	LKKR[d]	This work	Expt.
Rh				147	145	
Ir				243	217	
Ni				70	88	43[e]
Pd			97	76	106	
Pt					179	161[e]
Cu		29		36	26	24[f]
Ag		12		19	16	8[f]
Au		21		21	26	15[f]
Al	54	60[g] 74[h]	130	56	140	75[i]

[a] See Ref. 3.
[b] See Refs. 5 and 6.
[c] See Ref. 4.
[d] See Ref. 2.
[e] See Ref. 1.
[f] See Ref. 28.
[g] See Ref. 8.
[h] See Ref. 7.
[i] See Ref. 29.

TABLE III.   Intrinsic stacking-fault energy for the fcc transition metals.

|						
			E_{in} (mJ/m^2)			
Metal	APW[a]	Supercell pseudo[b]	LMTO[b]	LKKR[c]	This work	Expt.
Rh				308	320	750[d]
Ir				534	499	480[d]
Ni				180	187	125[d]
Pd				161	225	180[d]
Pt					393	322[d]
Cu		50	51	70	56	55[e] 48[f] 41[g]
Ag		18	38	33	34	22[e] 20[f] 16[h]
Au		45	52	44	59	50[e] 42[f] 32[i]
Al	126	156[j] 161[k]	280[l]	124	295	166[m]

[a] See Ref. 3.
[b] See Refs. 5 and 6.
[c] See Ref. 2.
[d] See Ref. 1.
[e] Values recommended by Gallager (Ref. 31).
[f] See Ref. 30.
[g] See Ref. 32.

[h] See Ref. 33.
[i] See Ref. 34.
[j] See Ref. 8.
[k] See Ref. 7.
[l] See Ref. 4.
[m] See Ref. 29.
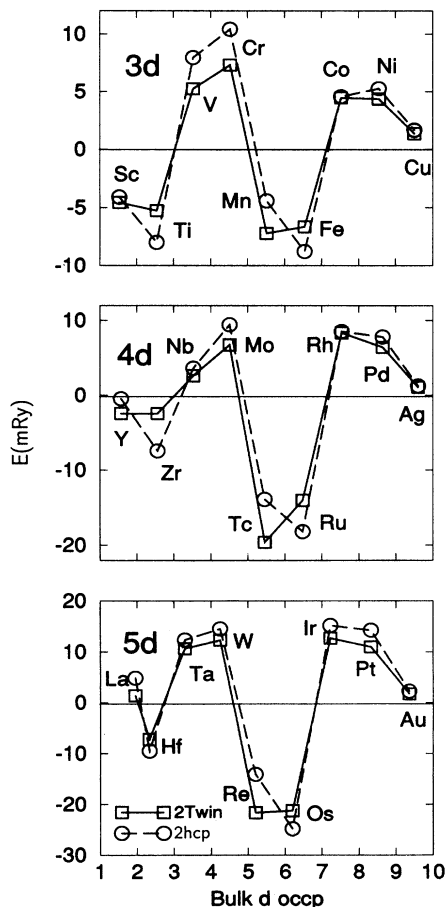
FIG. 2.   The calculated twin-fault energy of the 3d, 4d, and 5d transition metals compared to the structural energy differences between the hcp and fcc structures. Note that to comply with the approximate relations (21) and to make direct comparisons with the following figures we have plotted $2E_{\text{twin}}$ and $2E_{\text{hcp}}$.

In comparison with the LKKR results we find that for Rh and Ir the two sets of calculations agree to within 15% for all three stacking faults. For Ni the deviations are up to 25% and for the intrinsic fault in Pd the LKKR is lower than the corresponding value for Ni in contrast to both the present value and the experimental trend. In the case of the noble metals the deviation between the LKKR and the present results is up to 30%. However, both sets of calculations correctly describe the trend that the three fault energies for Ag are lower than the corresponding values for both Cu and Au. This is in agreement with the energy-band picture in which relativistic effects lead to a raising of the d band in Au relative to the s band leaving Ag with the lowest-lying d band of the three noble metals.

The supercell approach, in which the two-dimensional fault structure is treated by means of a conventional

TABLE IV.   Extrinsic stacking-fault energy for the fcc transition metals.

		E_{ex} (mJ/m^2)			
Metal	APW[a]	Supercell pseudo[b]	LMTO[c]	LKKR[d]	This work
Rh				282	291
Ir				494	440
Ni				149	178
Pd				156	214
Pt					374
Cu		44		73	57
Ag		18		38	35
Au		41		44	59
Al	108	138[e]151[f]	260	118	291

[a] See Ref. 3.
[b] See Refs. 5 and 6.
[c] See Ref. 4.
[d] See Ref. 2.
[e] See Ref. 8.
[f] See Ref. 7.

TABLE V. Calculated hcp structural energy difference and fcc stacking-fault energies in mRy for the 3d, 4d, and 5d transition metals.

	Sc	Ti	V	Cr	Mn	Fe	Co	Ni	Cu
E_{hcp}[a]	-1.82	-3.35	2.72	3.76	-2.08	-3.79	2.39	2.53	0.78
E_{hcp}[b]	-2.04	-4.00	3.97	5.19	-2.21	-4.39	2.28	2.63	0.83
E_{twin}[b]	-2.27	-2.63	2.62	3.66	-3.60	-3.32	2.22	2.18	0.67
E_{in}[b]	-4.10	-7.16	8.69	8.00	-4.97	-8.46	4.71	4.57	1.45
E_{ex}[b]	-4.14	-5.05	3.21	8.21	-7.54	-6.16	4.35	4.39	1.47
	Y	Zr	Nb	Mo	Tc	Ru	Rh	Pd	Ag
E_{hcp}[a]	-0.77	-2.80	0.93	2.63	-5.91	-6.65	4.70	3.65	0.51
E_{hcp}[b]	-0.22	-3.71	1.80	4.70	-6.96	-9.10	4.25	3.91	0.64
E_{twin}[b]	-1.21	-1.22	1.32	3.35	-9.81	-7.02	4.17	3.20	0.54
E_{in}[b]	-1.48	-5.49	5.87	6.60	-15.3	-17.8	9.19	6.76	1.13
E_{ex}[b]	-1.89	-1.47	0.00	7.27	-20.5	-13.2	8.36	6.45	1.16
	La	Hf	Ta	W	Re	Os	Ir	Pt	Au
E_{hcp}[a]	1.51	-4.71	4.32	5.00	-5.86	-7.95	8.22	6.86	0.92
E_{hcp}[b]	2.39	-4.76	6.19	7.28	-7.04	-12.4	7.60	7.14	1.11
E_{twin}[b]	0.67	-3.61	5.30	6.14	-10.8	-10.6	6.34	5.47	0.85
E_{in}[b]	2.96	-9.06	14.7	12.4	-16.4	-25.3	14.6	12.0	1.94
E_{ex}[b]	1.26	-6.48	7.29	13.6	-22.1	-19.6	12.9	11.4	1.93

[a]See Ref. 37.
[b]Present result.

three-dimensional one-electron method, has been applied in a number of cases. Xu, Lin, and Freeman[4] used the LMTO method within the ASA to calculate stacking-fault energies in Pd and Al, and the noble metals were studied by Schweizer and co-workers[5,6] by means of the LMTO method within the ASA, as well as by a non-shape-restricted pseudopotential method. The agreement at the 10% level between the LMTO supercell calculations and the present LMTO Green's-function results indicates that the perturbation generated by a stacking fault is extremely localized and hence may be treated to a high accuracy also by a supercell method.

All four ab initio calculations listed in Tables II–IV confirm the trend that Ag has the lowest stacking-fault energies among the noble metals. However, at the quantitative level there are large and unsystematic deviations between the calculations. If one considers the twin and intrinsic stacking faults, it appears that the pseudopotential calculation is in best agreement with the experimentally derived values. On the other hand, the pseudopotential result deviates more from the theoretically based relationship $E_{\text{in}} \approx E_{\text{ex}} \approx 2E_{\text{twin}}$ than does the LKKR and the present results. One reason for this deviation may be the limited size of the supercell, which could compromise the accuracy of the pseudopotential calculations.

In the case of Al, the supercell augmented plane wave (APW), the supercell pseudopotential, and the LKKR methods give stacking-fault energies which vary among each other by up to 40% but otherwise are in reasonable agreement with the experimentally derived values. In contrast to this, the supercell LMTO and the Green's-function calculations agree to within 10%, but

give stacking-fault energies which are almost a factor of 2 larger than the experimental values. One reason for this discrepancy may be the fact that the LMTO method within the ASA tends to be less accurate for metals with broad sp bands and relatively large electron density in the outer parts of the Wigner-Seitz cell.

B. Trends in the transition-metal series

The three types of stacking faults shown in Fig. 1 consist of a perfect fcc stacking sequence interrupted by one or two layers, which as far as the neighboring layers are concerned, have a hcp environment. The energies of these stacking sequences may be analyzed in terms of an Ising model[35,8] or a pair potential in conjunction with a tight-binding model.[36] With short-range interactions the models lead to the approximate relations

$$2E_{\text{hcp}} = 2E_{\text{twin}} = E_{\text{in}} = E_{\text{ex}}, \qquad (21)$$

where E_{hcp} is the structural energy difference between the hcp and the fcc structures. These relations may also be obtained in a nearest-neighbor layer model simply by counting the number of layers with a hcp environment in Fig. 1. The accuracy with which they are obeyed by the ab initio calculations may be judged from Table V and Figs. 2–4 and will in turn justify the localized models of stacking faults.

In Figs. 2 and 3 we have plotted the calculated twin and intrinsic stacking-fault energies together with the hcp structural energy differences also obtained in the present work for the 3d, 4d, and 5d transition metals. The comparison shows clearly the applicability of the two first
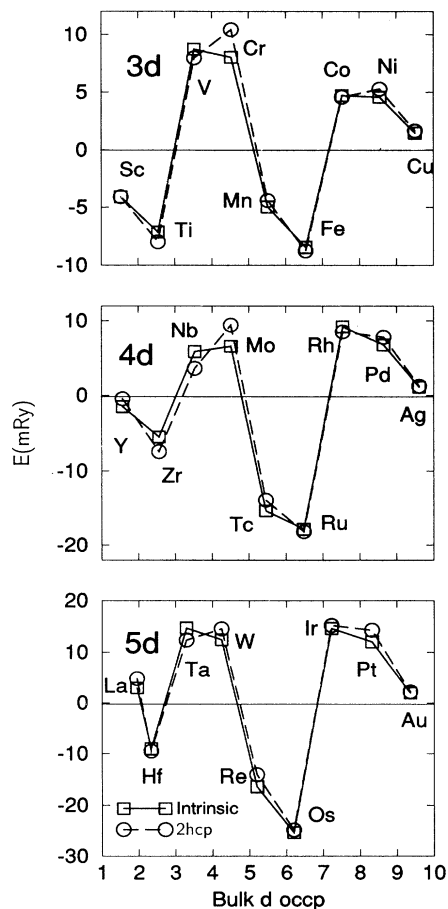
FIG. 3. The calculated intrinsic fault energy of the $3d$, $4d$, and $5d$ transition metals compared to twice the structural energy differences between the hcp and fcc structures.
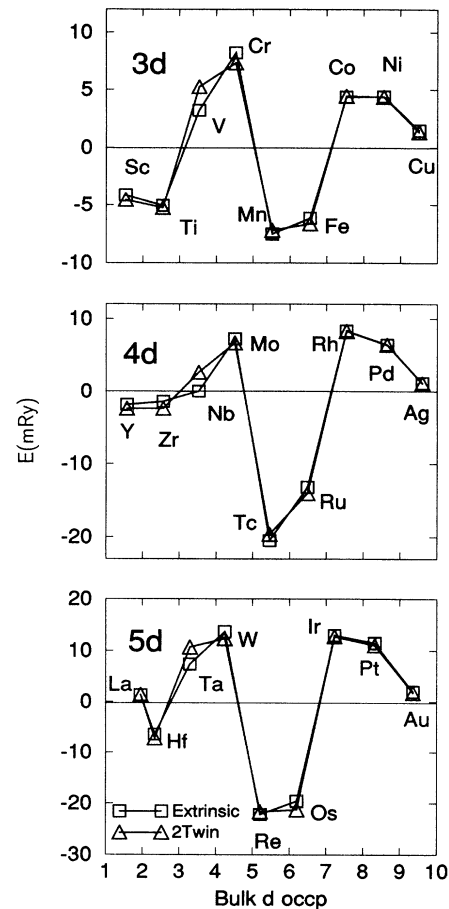

FIG. 4. The calculated extrinsic fault energy of the $3d$, $4d$, and $5d$ transition metals compared to twice the twin-fault energy.

relations in (21). In Fig. 4 we have compared the extrinsic and the twin-fault energies for the transition metals and find an almost perfect proportionality between the two. Apart from justifying the local interaction picture of stacking faults, the accuracy with which these relations are obeyed may serve as an internal consistency check on calculated as well as experimentally derived stacking-fault energies.

It is clear from Figs. 2–4 that the stacking-fault energies of the three transition series follow the same trend as a function of the calculated d occupation number. We have therefore plotted the calculated energies scaled by the appropriate d-band widths together with the results of a canonical d-band model for the hcp-fcc structural energy difference in Fig. 5. It is seen that the change in magnitude of the fault energies in the $3d$, $4d$, and $5d$ metals to a large degree is caused by the increase in the d-band width. It is furthermore seen that the canonical d-band model, which relies only on the crystal structure and not on the atomic potentials, gives a correct qualitative description of the fault energies. Thus, we conclude that the d band to a large degree controls the formation of stacking faults. However, it is also clear that the hy-
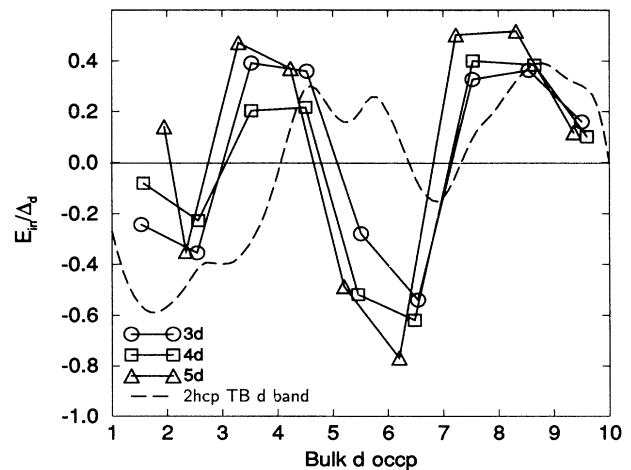

FIG. 5. The calculated intrinsic fault energy of the $3d$, $4d$, and $5d$ transition metals scaled by the calculated d-band width Δ_d and compared to the results of a tight-binding canonical d-band model.

bridization with the sp band cannot be neglected if one wants a quantitative model.

We note from Table V that the agreement between the fault energies and the hcp structural energy differences is less satisfactory if we use the hcp energies calculated by Skriver.[37] Such a comparison is, however, slightly inconsistent since he used a third-order LMTO-ASA Hamiltonian and included combined correction terms. It may, on the other hand, serve as a check on the accuracy of the second-order tight-binding LMTO Hamiltonian used in the Green's-function technique. We find that, for the proper fcc metals at the right-hand side of the Periodic Table, the application of the second-order Hamiltonian leads to errors of less than 10%.

IV. CONCLUSION

We have calculated the twin, intrinsic, and extrinsic fcc stacking-fault energies for the 3d, 4d, and 5d transition metals. The values confirm a series of simple relations between these energies and the energy difference between the hcp and the fcc structure and thereby justify the lo-

cal model for stacking faults. The present values for the fault energies of the proper fcc metals at the right-hand side of the Periodic Table are in good agreement with previous *ab initio* calculations and are in semiquantitative agreement with experiments. Here, one should note that the experimental stacking-fault energies are derived in an indirect way, and in some cases one has even made use of theoretical relations such as those given in Eq. (21) to obtain experimental values. One may therefore argue that present day *ab initio* calculations may be the most consistent method of obtaining stacking-fault energies.

ACKNOWLEDGMENTS

[1] J.P. Hirth and J.L. Lothe, *Theory of Dislocations* (Wiley, New York, 1982).

[2] S. Crampin, K. Hampel, D.D. Vvedensky, and J.M. Maclaren, J. Mater. Res. **5**, 2107 (1990).

[3] P.J.H. Denteneer and J.M. Soler, J. Phys. Condens. Matter **3**, 8777 (1991).

[4] J.-H. Xu, W. Lin, and A.J. Freeman, Phys. Rev. B **43**, 2018 (1991).

[5] S. Schweizer, C. Elsässer, K. Hummler, and M. Fähnle, Phys. Rev. B **46**, 14 270 (1992).

[6] M. Fähnle, S. Schweizer, C. Elsässer, and A. Seeger (unpublished).

[7] A.F. Wright, M.S. Daw, and C.Y. Fong, Philos. Mag. A **66**, 387 (1992).

[8] B. Hammer, K.W. Jacobsen, V. Milman, and M.C. Payne, J. Phys. Condens. Matter **4**, 10 453 (1992).

[9] H.L. Skriver and N.M. Rosengaard, Phys. Rev. B **43**, 9538 (1991).

[10] H.L. Skriver and N.M. Rosengaard, Phys. Rev. B **45**, 9410 (1992).

[11] H.L. Skriver and N.M. Rosengaard, Phys. Rev. B **46**, 7157 (1992).

[12] M.E. Aldén, S. Mirbt, H.L. Skriver, N.M. Rosengaard, and B. Johansson, Phys. Rev. B **46**, 6303 (1992).

[13] O.K. Andersen, Phys. Rev. B **12**, 3060 (1975).

[14] O. Gunnarsson, O. Jepsen, and O.K. Andersen, Phys. Rev. B **27**, 7144 (1983).

[15] H.L. Skriver, *The LMTO Method* (Springer-Verlag, Berlin, 1984).

[16] O.K. Andersen and O. Jepsen, Phys. Rev. Lett. **53**, 2571 (1984).

[17] O.K. Andersen, O. Jepsen, and D. Glötzel, in *Highlights of Condensed-Matter Theory*, edited by F. Bassani, F. Fumi, and M.P. Tosi (North-Holland, New York, 1985).

[18] O.K. Andersen, Z. Pawlowska, and O. Jepsen, Phys. Rev. B **34**, 5253 (1986).

[19] W.R.L. Lambrecht and O.K. Andersen, Surf. Sci. **178**, 256 (1986); (private communication).

[20] A.R. Williams, P.J. Feibelman, and N.D. Lang, Phys. Rev. B **26**, 5433 (1982).

[21] F. Garcia-Moliner and V.R. Velasco, Prog. Surf. Sci. **21**, 93 (1986).

[22] J. Kudrnovský and V. Drchal, *Studies in Surface Science and Catalysis*, edited by J. Koukal (Elsevier, Amsterdam, 1988), Vol. 36, p. 74.

[23] B. Wenzien, J. Kudrnovský, V. Drchal, and M. Šob, J. Phys. Condens. Matter **1**, 9893 (1989).

[24] S.L. Cunningham, Phys. Rev. B **10**, 4988 (1974).

[25] D.M. Ceperley and B.J. Alder, Phys. Rev. Lett. **45**, 566 (1980).

[26] J. Perdew and A. Zunger, Phys. Rev. B **23**, 5048 (1981).

[27] J.M. MacLaren, S. Crampin, D.D. Vvedensky, and M.E. Eberhardt, Phys. Rev. B **40**, 12 164 (1989).

[28] L.E. Murr, Scr. Metall. **6**, 203 (1972).

[29] L.E. Murr, Acta Metall. **21**, 791 (1973).

[30] P.C.J. Gallager and Y.C. Liu, Acta Metall. **17**, 127 (1969).

[31] P.C.J. Gallager, Metall. Trans. **1**, 2429 (1970).

[32] W.M. Stobbs and C.H. Sworn, Philos. Mag. **24**, 1365 (1971).

[33] D.J.H. Cockayne, M.L. Jenkins, and I.L.F. Ray, Philos. Mag. **24**, 1383 (1971).

[34] M.L. Jenkins, Philos. Mag. **26**, 747 (1972).

[35] C. Cheng, R.J. Needs, and V. Heine, J. Phys. C **21**, 1049 (1988).

[36] K. Stokbro and K.W. Jacobsen, Phys. Rev. B **47**, 4916 (1993).

[37] H.L. Skriver, Phys. Rev. B **31**, 1909 (1985).